ARCHIVES OF ELECTRICAL ENGINEERING VOL. 62(2), pp. 195-207 (2013)

DOI 10.2478/aee-2013-0015

Comparison of numerically determined noise of a 290 kW induction motor using FEM and measured acoustic radiation

MASEN AL NAHLAOUI, HENDRIK STEINS, STEFAN KULIG, SVEN EXNOWSKI

Institute of Electrical Machines and Mechatronics
TU Dortmund University
Emil Figge Str. 70, 44227 Dortmund

e-mail: masen.nahlaoui@tu-dortmund.de

(Received: 17.06.2012, revised: 05.11.2012)

Abstract: In this paper a comparison of numerically determined and measured electromagnetically exited noise of an induction motor is presented. The calculations are accomplished using FEM for an example motor, which is a 290 kW inverter-fed asynchronous machine. The approach starts with the electromagnetic and mechanical consideration. The focus is set on acoustic considerations, which contain the 3D-FE-model and measurement setup in the sound chamber.

Key words: inverter-fed, induction motor, asynchronous machine, acoustic radiation, modal analysis

1. Introduction

Calculating the noise emission of electrical machines has been very important for decades now. In [5, 8] for example basic considerations and efforts to deduce the noise emission have been performed. The air-gap field has also been investigated in [1, 4, 7]. However, the increasing use of inverters has drastically increased the relevance of these investigations. Up to now, the calculation has been based on analytical methods. However, to establish the transient behavior and to take the geometry and non-linearities into account, it is necessary to use the finite element method.

In the first step, the electromagnetic model and calculation of the forces acting on the stator core are described. The forces are presented as rotating force waves up to 10 kHz. A distinction is made between feeding the motor with sinusoidal and inverter currents.

The second step presents a three dimensional mechanical model, which is used to calculate the surface vibration of the machine. This is a very detailed model, including stator core, slot filling, shields and enclosure. Verification has been done by comparing numerical and experimental modal analyses. An extract of the measurement results is presented.

The third step deals with the acoustic 3D FE calculations and the comparison between the calculated and measured noise emission of the asynchronous machine.

2. Electromagnetic considerations

The determination of induction and force waves up to 10 kHz requires a well-designed modeling. Especially the air-gap needs a very fine mesh, which is able to build up the rotor steps at the chosen time step of 5 µs. This can easily result in a huge computational effort. Figure 1 shows the electromagnetic model in Flux2D to calculate the force waves up to 10 kHz.

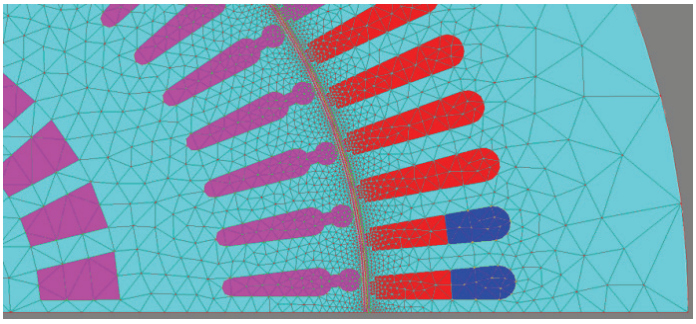

Fig.1. Electromagnetic model to calculate the force waves up to 10 kHz

This model includes nearly fifty thousand nodes, and as can be seen in the diagram, the air gap has a very fine mesh.

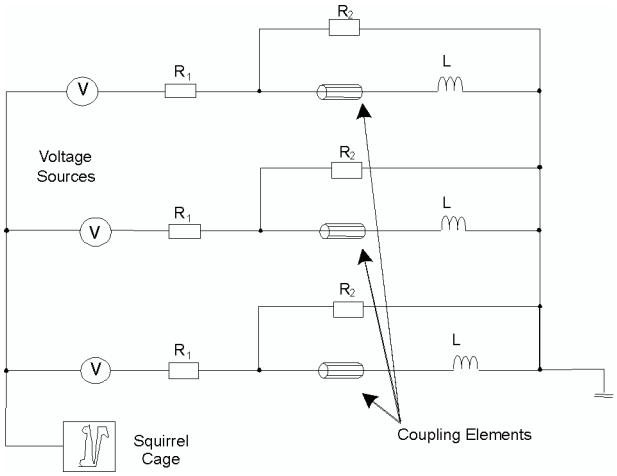

Fig. 2. Coupling circuit to inject any voltage curve

It is also important to couple the FE domain to an additional network as shown in Figure 2. This network is used to realize different types of feedings for the asynchronous machine, inverter-feeding or sinusoidal voltage source-feeding. In Figure 2 the sinusoidal voltage source-feeding is presented. The resistance of each phase can be specified in the coupling elements. The series-connected inductances include the end winding inductance. Resistances R are just elements to simplify the post processing.

It is necessary to use a transient calculation to take the rotor rotation into account. This simulation leads to the induction in the middle of the air-gap as a curve over the time and location in the air-gap. Using the two-dimensional Fourier-Transformation it is possible to decompose the curve into radial induction waves [2], which can be analysed.

For the resulting matrix B_{rad} a two-dimensional fast Fourier transformation is performed. Therefore, different basics of frequency analysis are needed [2]. The transformation of the columns results in the frequency peaks, whereas the lines result in the harmonic number on the circumference. For example, a wave described by $f = 50$ Hz and $r = 2$ is a wave with two full sine waves on the circumference and every point oscillates at 50 Hz. The result is a rotating wave.

Table 1 shows the induction waves in the air gap, which are caused by the stator when fed by a sinusoidal voltage source. The comparison is made between rated and no-load operation. Amplitudes are given in percent based on the fundamental for rated operation. Only amplitudes larger than 1% of the fundamental are considered. Two categories of waves can be seen. Those with a frequency of 50 Hz are caused by the stator winding and slots. The harmonic number is given by [1]

$$\nu_1 = p \cdot (6n + 1), \text{ where } n \in Z \setminus \{0\}. \tag{1}$$

In this formula p is the number of pole pairs. The most pronounced waves are those that also contain the slot harmonics, where the slot number is 72. In addition to the 50 Hz waves, 150 Hz and 250 Hz waves can be seen. These represent the 3rd and 5th saturation harmonics. In analytical considerations, usually just the 3rd order wave is calculated. The calculation shows that this is not a valid simplification, because the 5th order wave has similar amplitude to the 3rd.

The comparison of the two operating conditions shows that most waves – except the fundamental and slot harmonics – decrease by almost 50 %.

Table 2 shows the waves that are caused by the rotor. The harmonics can be categorized in

- rotor slot fields,
- rotor winding fields,
- residual rotor fields.

Where ν_2 is the harmonic number of the wave, which is given by [1]

$$\nu_2 = p + k_2 N_2, \text{ where } k_2 \in Z \setminus \{0\}. \tag{2}$$

In these equations, f_1 is the frequency of the current fed to the motor, N_2 the number of rotor bars and s the slip. The induction waves, whose frequency vary from these can be identified as residual rotor fields.

Table 1. Induction air gap waves caused by the stator using sinusoidal voltage sources under rated and no-load operation. Amplitudes are given in percent based on the fundamental for rated operation

Harmonic number r [ ]	**Frequency f [Hz]**	**B_{rad} rated operation [%]**	**B_{rad} no-load operation [%]**	**Deviation for no-load operation [%]**
2	50	100.00	102.17	2.17
10	50	2.58	1.50	−41.78
14	50	1.70	0.87	−48.89
26	50	1.25	0.66	−46.88
34	50	1.65	0.83	−49.62
38	50	1.60	0.80	−49.97
62	50	1.62	0.86	−47.10
70	50	14.99	12.57	−16.15
74	50	9.55	7.33	−23.21
142	50	6.46	6.51	0.80
146	50	5.01	5.28	5.52
6	150	1.30	0.74	−43.10
10	250	1.47	1.19	−19.11

These result from the induced fields with respect to each field that is applied to the rotor. These can be calculated using [1]

$$v_2 = v_1 + k_2 N_2, \tag{3}$$

$$f_{v_2} = f_{v_1} + \frac{k_2 N_2}{p} \cdot (1 - s) \cdot f_1, \tag{4}$$

where $k_2 \in Z \setminus \{0\}$. Further v_1 and f_{v_1} are the frequency and harmonic number of the exciting stator induction wave.

The previous results give an impression of which waves are expected and the influence of the actual operating condition. The influence of the inverter is now considered. Overall, the waves which have already been shown do not vary significantly. Because of this fact, the focus will be on the additional induction waves. The inverter is pulsed with 1250 Hz under no-load operating conditions.

Table 2 shows the relationship between the two largest current harmonics caused by the inverter and the resulting induction waves. Although these two currents have amplitudes of approximately 9% of the fundamental, the resulting waves only reach about 0.5%. This is caused by the induction in the rotor cage. On one hand, the high frequency leads to higher induction. On the other hand high frequency waves rotate faster so that the slip is nearly equal

to one. For example, harmonic simulation using a current source has shown that at same current amplitude and same mechanical rotational speed, but for a current frequency of 1150 Hz instead of 50 Hz, only a 6.5% air gap induction is obtained. Although these waves are very small, as the force waves are calculated by multiplying the induction waves, many more force waves are obtained than when compared to sinusoidal currents. This will be shown in the next chapter.

Table 2. Induction air gap waves caused by the inverter under no-load operating condition. Amplitudes are given in percent based on the fundamental

Frequency f [Hz]	**Current amplitude [%]**	**Harmonic number r [ ]**	**Direction of rotation**	**B_{rad} [%]**
50	100.00	2	1	100.00
1150	9.00	2	−1	0.25
		10	1	0.19
		14	−1	0.13
		70	1	0.40
		74	−1	0.35
1350	8.70	6	−1	0.41
		6	1	0.35
		30	−1	0.17
		30	1	0.15
		66	−1	0.28
		66	1	0.36
		78	−1	0.17

The comparison of rated and no-load operation as well as consideration of inverter-fed has been presented in [6]. Further the calculation of the force waves using Maxwell's stress tensor and the transition to the mechanical model has been shown in [6], too.

3. Mechanical considerations

To determine the surface vibrations, which are the input values for the following acoustic calculation, it is necessary to build up a three-dimensional structural model (Fig. 3). This model is very detailed to approximate the real vibrational behavior of the machine very well.

Modal analysis is one of the most important methods to verify models in different disciplines. In this case, a three dimensional finite element modal analysis has been performed for rigid and soft foundations. For these two cases, an experimental modal analysis has also been performed. Additionally, a comparison of the measurement was made, including stator

core, winding and housing with measurements taking only the shields or shields and rotor into account.

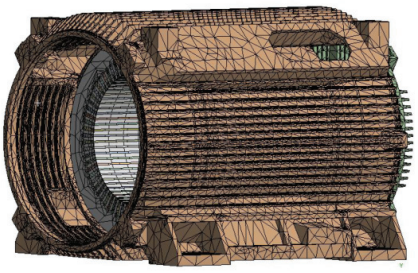

Fig. 3. Mechanical FE-model

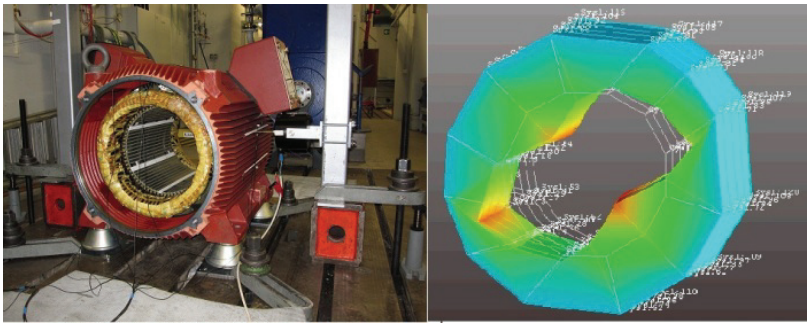

Fig. 4. Experimental modal analysis. Test setup and $r = 2$, $n = 0$ mode visualized in the measurement model

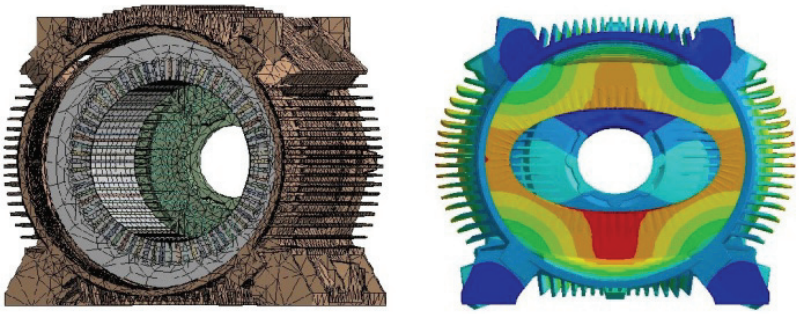

Fig. 5. Numerical modal analysis. Model and $r = 2$, $n = 0$ mode visualized in ANSYS

Figure 4 shows the test setup. The vibrations have been measured on the teeth at 35 points and outside on the enclosure ribs at 35 more points. To visualize the results a model had to be programmed in the software. The model and the $r = 2$, $n = 0$ mode can also be seen in Figure 5. It contains 12 nodes on the circumference, of which 7 are really measured (master) nodes. The 5 other nodes are interpolated slave nodes to refine the visualization. 5 planes are measured in axial direction.

Table 3 shows the natural frequencies of the modes being considered in the case of a rigid foundation and the difference between the numerical and experimental results – taking the shields and rotor into account. It can be seen that the frequencies are in a maximum tolerance band of 17%. Further, the $r = 0$ modes are in a band of 3%.

Table 3. Comparison of the natural frequencies determined with the numerical and experimental modal analysis for a rigid foundation The frequencies are given in p.u. based on the FE Eigen frequency of the $r = 2$, $n = 0$ mode. This is the mode with the lowest frequency

Mode shape	**FE results [p.u.]**	**Measurement including rotor [p.u.]**	**Difference [%]**
$r = 0,\ n = 1$	4.30	4.15	−3.5
$r = 0,\ n = 2$	4.85	4.83	−0.53
$r = 2,\ n = 0$	1.00	0.90	−9.54
$r = 2,\ n = 1$	1.61	1.34	−16.67
$r = 3,\ n = 0$	2.43	2.06	−15.16
$r = 3,\ n = 1$	3.55	3.25	−8.37

The previous results and comparison show that the mechanical model delivers very good results. Remarkable is that for the $r = 0$, $n = 2$ mode the deviation is less than 1%. These results lead to the conclusion that the FE-model approaches the real vibrational behavior of the machine very well and is used to determine the surface vibration for the following acoustic simulations.

The next section discusses the calculation of the surface vibrations.

Up to now, only the radial waves of the flux density have been evaluated. This simplification can be made as the tangential component of the flux density is less than 10% of the radial component. Another aspect is the very small air gap, which reinforces an approximately pure radial field. The force density can be calculated from this using the Maxwell stress tensor in [4]

$$\sigma_{rad} = \frac{{B_{rad}}^2}{2\mu_0}. \tag{5}$$

This shows that if the air gap field is described by the sum of many induction waves, the whole sum has to be squared to calculate the force waves. The force calculation can be determined from this as follows

$$\sigma_{rad} = \frac{1}{2\mu_0} \cdot \left[\sum_i \left(\hat{B}_t \cdot \sin\left(2\pi f_i \cdot t + r_i \cdot x\right) + \phi_i \right) \right]^2, \tag{6}$$

This equation shows that also induction waves with small amplitudes can lead to significant force waves, if they are multiplied by an induction wave with large amplitude. To avoid errors caused by limiting the induction waves to a minimum peak height, the whole transient 3D curve is squared and Fourier transformed.

The forces were impressed on the outer edges of each of the 72 teeth. This results in 144 interpolation points to build up each wave. For example, to impress a 100 Hz, $r = 4$ force wave, every line is allocated the same amplitude, but the phase is distributed by

$$\varphi = r \cdot x, \tag{7}$$

where x is the position on the circumference. Figure 5 shows the distribution for the wave mentioned above. In this diagram, x is replaced by the line number on which the force is impressed. The lines are in the same order as the position on the circumference.

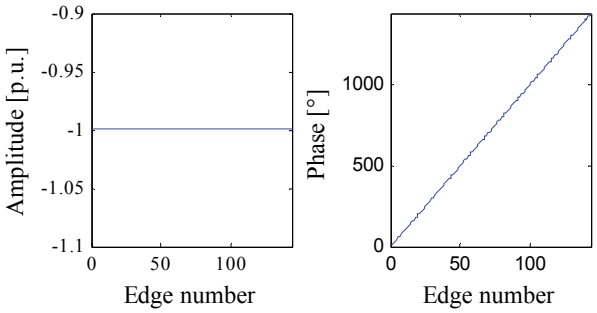

Fig. 5. Amplitude and phase of the forces to impress an r = 4 rotating force wave. Each tooth has two edges. A force is impressed on each edge. For 72 teeth, this results in 144 edges or interpolation points

But as the consideration of the force waves has shown, it is possible that several force waves with different harmonic order exist at one frequency. To impress the sum of these waves, all waves with the same frequency – but different areal harmonic numbers – have to be summed complex. This leads to different amplitudes at each point and different phases. The sum is the desired superposition. The resulting distribution is shown in Figure 6, as example for the sum of the following three force waves:

Harmonic number r [ ]	Frequency f [Hz]	Amplitude [p.u.]
0	100	0.75
4	100	1.00
16	100	0.50

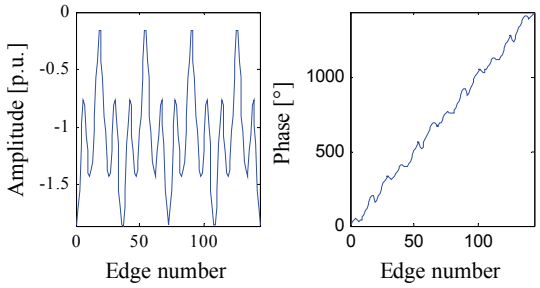

Fig. 6. Amplitude and phase of the forces to impress $r = 4$, $r = 16$ and $r = 0$ rotating force waves

If the forces were to now be considered in the complex plane, the force vector would not move on a circle, but on a pattern which is shown in the following Figure 7.

This method to impress the force waves can be applied to a 3D or 2D model. The only difference is to impress the forces on the outer points or outer lines of each tooth.

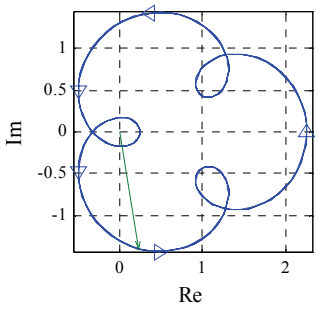

Fig. 7. The pattern along which the force vector moves seen on the circumference for the sum of $r = 4$, $r = 16$ and $r = 0$ rotating force waves

A few possibilities can be considered in order to analyse the result. On one hand a Fourier transformation in the different planes can be performed. On the other hand, a modal decomposition could be useful to describe the excited mode shapes. Further, a comparison between the two-dimensional results, which are calculated without enclosure, can be made.

In addition to these considerations, which are based on the two and three-dimensional curves, the vibration of the whole machine including enclosure can be visualized.

Figure 8 shows the resulting deformation under no-load operation, and when fed by an inverter and by a sinusoidal source. It can be seen that the deformation is different. However this deformation consists of the superposition of many deformations. Especially at high frequencies, a small deformation can lead to unpleasant noise emission, because the sound particle velocity is crucial.

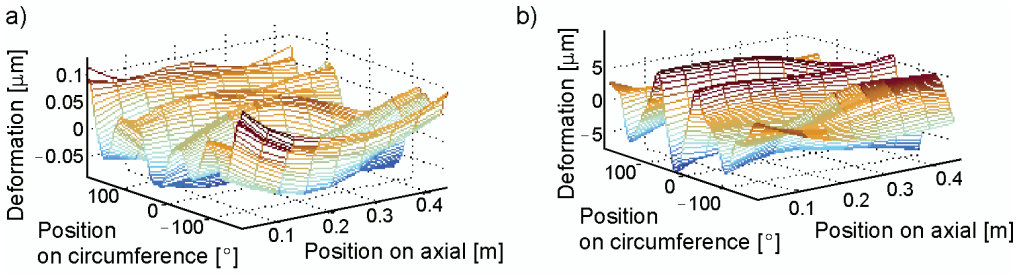

Fig. 8. Deformation at all frequencies on the outer circumference of the stator core under no-load operation except the 100 Hz component for: a) when fed by an inverter, b) when fed by a sinusoidal source

Figure 9 shows the forced mode shape at 3100 Hz when fed by an inverter. This diagram shows an example of one of the many excited mode shapes.

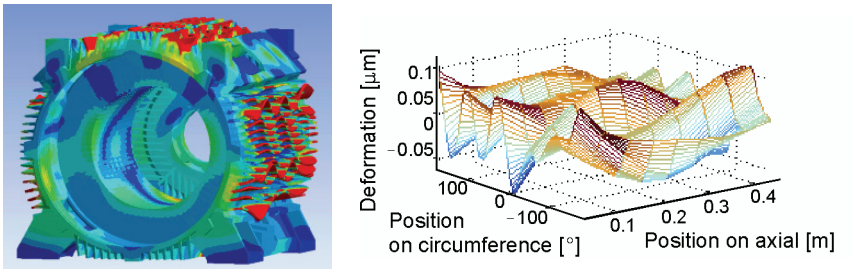

Fig. 9. Forced mode shape at 3100 Hz when fed from an inverter

4. Acoustic Considerations

Even for the acoustic considerations, very detailed measurements have been accomplished. The example motor has been measured in no-load operation for sinusoidal voltages and inverter-fed motor. Further weak foundation (Fig. 10a) and rigid foundation (Fig. 10b) has been considered. The measurement has been performed using the enveloping surface method according to ISO 3744. Therefor 14 microphones have been used.

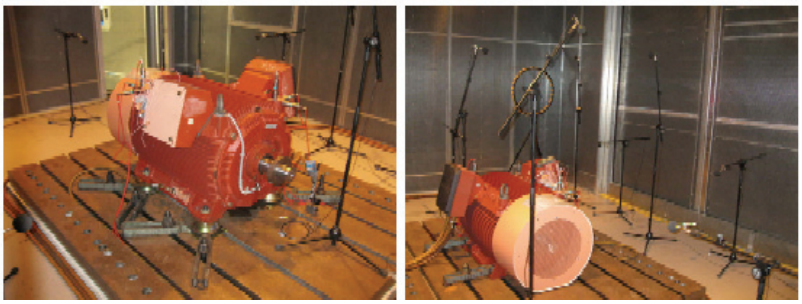

a) weak foundation b) rigid foundation

Fig. 10. Measurement setup in the sound chamber

Figure 11 presents the Campbell diagram for no-load operation and with sinusoidal voltages fed motor. The sound pressure level is visualized using the colorbar whereas the frequency and rotational speed are shown on *x*-axis respectively on *y*-axis. The red diagonal progressions display the noise components which depend on the rotational speed.

Comparing the results of Figure 12 to the results of Figure 11 it becomes obvious that the influence of the inverter is visible. The pre-existing components are still present but with a lower amplitude. In addition more or less vertical bars with clearly higher amplitude are visible at the inverter clocking frequency and it's multiple.

In Figure 13 the model used to calculate the noise emission in different bands up to 10 kHz is presented. The size of the shown enveloping body has to be the minimum of either to factor 0.5 larger than the calculated body, or the maximum considered wavelength. Therefore to re-

duce the calculation time the frequency band has been split in 0-2 kHz, 2-5 kHz and 5-10 kHz. Furthermore the model consists of a coupling surface, which is the surface of the motor. Based on this the finite element domain is defined, which is the enveloping body. Then on the enveloping body infinite elements are chosen. Last the post mesh or any points are set as microphones.

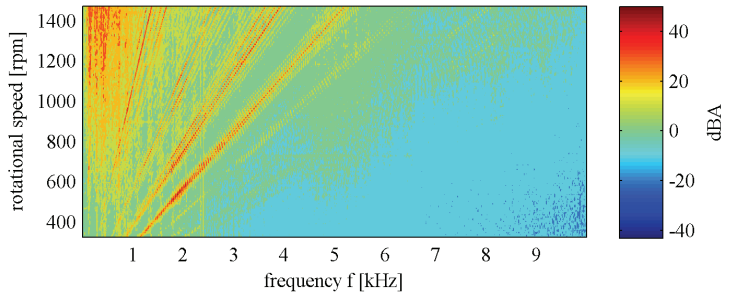

Fig. 11. Measured sound pressure level dependent on the rotational speed and sound frequency for sinusoidal voltages

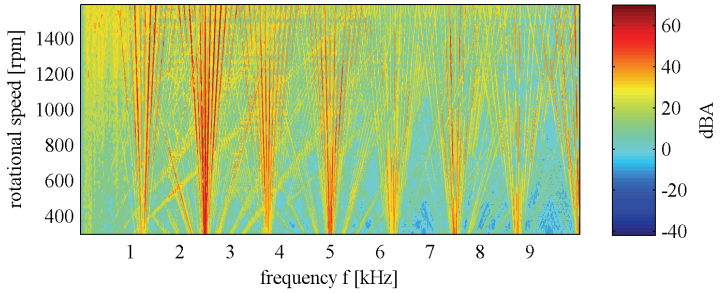

Fig. 12. Measured sound pressure level dependent on the rotational speed and sound frequency for inverter-fed motor at 1250 Hz inverter clocking

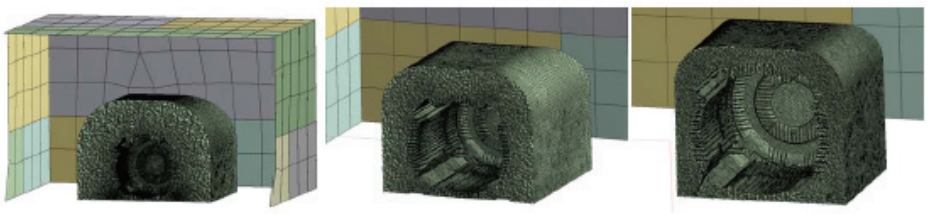

a) 0-2 kHz b) 2-5 kHz c) 5-10 kHz

Fig. 13. Acoustic FE-models for the three frequency bands

Finally numerical results of the radiated noise are compared to the measured noise. This is presented for inverter-fed machine at no-load operation in Figure 14. It can be seen that in sum

a good agreement results over a wide frequency band. Some amplitudes are determined too low because of the neglected tangential component of the force.

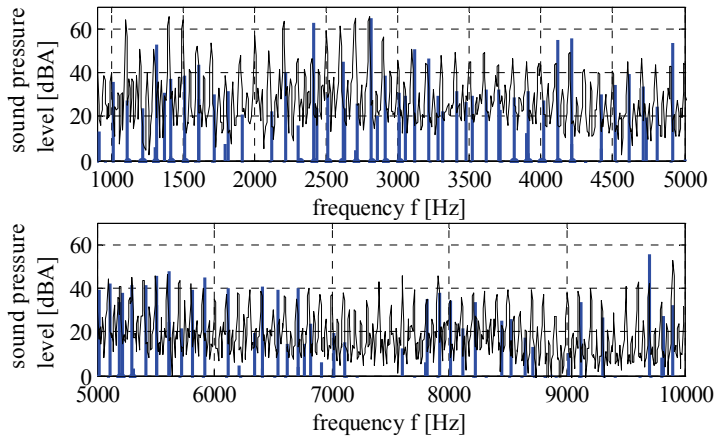

Fig. 14. Comparison of the measured noise (black line) and for discrete frequencies numerically determined noise (blue bars)

5. Conclusion

The previous sections have shown that the calculation of radial force waves can be performed with an acceptable effort. Transient simulations are required, which allow any current curves to be obtained. To allow a comparison between different cases or to analytical calculations, the transient curves have to be transformed into force and induction waves.

For the mechanical part, the modal analysis has shown that the created model is close to the real machine.

At last the acoustic considerations have shown that the numerical results lead to a good agreement to the measured noise. This follows that in future the FEM can be used more often to design new prototypes.

References

[1] Müller G., Ponick B., *Theorie of Electrical Machines, (Theorie elektrischer Maschinen)*. WileyVCH (2009).

[2] Hoffmann R., *Bases of Frequency Analysis, (Grundlagen der Frequenzanalyse)*. Expert Verlag, (2001).

[3] Nahlaoui M.Al., *Natural Frequencies and Vibration Behavior of an Asynchronous Machine, (Eigenfrequenzen und Schwingungsverhalten einer Asynchronmaschine)*. TU Dortmund University (2008).

[4] Seinsch H.O., *Higher Harmonic Phenomena of Rotary Field Machines, (Oberfeld Erscheinungen in Drehfeldmaschinen)*. B.G. Teubner Stuttgart (1992).

[5] Frohne H., *On the Primary Determinants of the Volume of Asynchronous Machines*, Technical University of Hanover (1959).

[6] Al Nahlaoui M., Kulig S., Werner U., *Electromechanical Forces and Vibration of an Asynchronous Machine for Sinusoidal and Inverter Currents*, 12th Portuguese-Spanish Conference on Electrical Engineering (2011).
[7] Al Nahlaoui M., Braunisch D., Eichinger B., Kulig S., Ponick B., Werner U., *Calculation Methods for Electromagnetically Excited Noise in Induction Motors.* 1st International Electric Drives Production Conference and Exhibition (2011).
[8] Jordan H., *Low Noise Electric Motors.* Verlag W. Girardet Essen (1950).